SGS Reaction rate modelling for MILD combustion based on machine-learning combustion mode classification

Development and a priori study

Jigjid, Kherlen; Minamoto, Yuki; Khoa Doan, Nguyen Anh; Tanahashi, Mamoru

DOI
10.1016/j.proci.2022.07.020

Publication date
2022

Document Version
Final published version

Published in
Proceedings of the Combustion Institute

Available online at www.sciencedirect.com

ScienceDirect

Proceedings of the Combustion Institute 39 (2023) 4489–4499

Proceedings of the Combustion Institute

www.elsevier.com/locate/proci

SGS Reaction rate modelling for MILD combustion based on machine-learning combustion mode classification: Development and a priori study

Kherlen Jigjid [a], Yuki Minamoto [a,b,*], Nguyen Anh Khoa Doan [c], Mamoru Tanahashi [a]

[a] *Department of Mechanical Engineering, Tokyo Institute of Technology, Meguro, Tokyo, 152-8550, Japan*
[b] *Japan Science and Technology Agency PRESTO, 7 Chiyoda, Tokyo 102-0076, Japan*
[c] *Faculty of Aerospace Engineering, Delft University of Technology, Kluyverweg 1, HS Delft 2629, Netherlands*

Received 2 January 2022; accepted 3 July 2022
Available online 4 August 2022

Abstract

A neural network (NN) aided model is proposed for the filtered reaction rate in moderate or intense low-oxygen dilution (MILD) combustion. The framework of the present model is based on the partially stirred reactor (PaSR) approach, and the fraction of the reactive structure appearing in the PaSR is predicted using different NN's, to consider both premixed and non-premixed conditions while allowing the use of imbalanced training data between premixed and non-premixed combustion direct numerical simulation (DNS) data. The key ingredient in the present model is the use of local combustion mode prediction performed by using another NN, which is developed in a previous study. The trained model was then assessed by using two unknown combustion DNS cases, which yields much higher dilution level (more intense MILD condition) and higher Karlovitz number than the DNS cases used as training data. The model performance assessment has been carried out by means of the Pearson's correlation coefficient and mean squared error. For both the present model and zeroth-order approximated reaction rate, the correlation coefficient with the target values shows relatively high values, suggesting that the trend of predicted field, by the present model and zeroth-order approximation, is well correlated with the actual reaction rate field. This suggests that the use of PaSR equation is promising if the fraction of the reactive structure is appropriately predicted, which is the objective in the present study. On the other hand, substantially lower mean squared error is observed for a range of filter sizes for the present model than that for the zeroth-order approximation. This suggests that the present filtered reaction rate model can account for the SGS contribution reasonably well.

Keywords: SGS Reaction rate modelling; MILD Combustion; Combustion mode; Machine learning; Direct numerical simulation (DNS)

* Corresponding author at: Department of Mechanical Engineering, Tokyo Institute of Technology, Meguro, Tokyo, 152-8550, Japan. *E-mail address:* yminamot@navier.mes.titech.ac.jp (Y. Minamo

https://doi.org/10.1016/j.proci.2022.07.020

1. Introduction

Due to ever-increasing energy demand and environmental issues in the world, more stringent regulations are constantly being applied to combustion devices and their operations. In particular, realisation of higher efficiency and less pollutant emission is considered to be the major requirement for future combustion devices.

One of the promising technologies that can meet upcoming regulations is moderate or intense low-oxygen dilution (MILD) combustion [1–3]. MILD combustion is realised with a combination of preheating and dilution of the reactant gas, and it can be achieved with either exhaust gas recirculation (EGR) or flue gas recirculation (FGR) configuration. The reactant gas is diluted and peak combustion temperature is reduced. Lower combustion temperature helps to reduce thermal NOx formation significantly [3]. Also, due to the recirculation, higher thermal efficiency is achieved. In typical MILD combustion, the unburnt gas temperature T_u is preheated higher than the autoignition temperature T_{ign}. Thus, the reaction is sustained even under highly diluted condition [2]. Furthermore, the temperature rise $\Delta T = T_b - T_u$ in MILD combustion is lower than T_u, where T_b is the burnt temperature [3]. Such small ΔT forms a relatively uniform combustion field and reduces combustion instabilities [1,2].

Large eddy simulations (LES) of MILD combustion are useful for design and optimisation of MILD combustion devices and operation conditions for industrial applications. In LES, coarse grid is considered and grid scale (GS) phenomena are explicitly resolved by solving the spatially-filtered transport equations. On the other hand, phenomena at the scale of subgrid scale (SGS) need to be modelled with SGS models. In this manner, LES can capture unsteady reacting flow structure with relatively low computational cost, although the LES results are highly dependent on the chosen models. In turbulent combustion LES, the most important SGS model is perhaps SGS turbulent combustion model, which predicts SGS interaction of turbulence and chemical reactions. Several SGS turbulent combustion models are proposed for MILD combustion [4–8]. However, due to its complex reaction zone characteristics described below, on top of usual turbulence–flame interaction, the SGS prediction is not straightforward.

Various experimental and numerical studies have been carried out to investigate the physics of MILD combustion. Direct photographs of MILD combustion and some advanced laser measurements of temperature and CH_2O fluorescence show uniformly distributed reaction zones [9–12]. However, clear flame fronts are also observed in OH planar laser induced fluorescence (PLIF) images [9–11,13]. Direct numerical simulation (DNS) results of MILD combustion with premixed and partially premixed reactants suggest the coexistence of flamelet-like reaction regions and distributed reaction region depending on the local thermochemical and turbulence conditions [14–16]. The flamelet type reaction region represents typical propagating flame; hence it is named “propagation mode” in the present study. On the other hand, distributed reaction region is formed due to flame-flame interaction or localised ignition of the reactant gas, and because of that it is named “ ignition/interaction mode”. The two combustion modes could be potentially important factors to be considered for the SGS turbulent combustion model for MILD combustion.

To include chemical and turbulence interactions, partially stirred reactor (PaSR) approach was suggested for LES of MILD combustion in previous studies, and shown to be effective [7,8]. The PaSR approach assumes the single numerical cell of LES to have both reactive structure and non-reactive surrounding fluid at the same time [17]. The reaction rate of the reactive structure can be calculated with a perfectly stirred reactor (PSR) or plug flow reactor (PFR). Meanwhile, the fraction of the reactive structure is obtained with a pair of characteristic chemical and mixing timescales [18]. The timescales can be chosen from a range of definitions. However, there is no proven method to choose the best pair of timescales, even though the choice affects the result of the simulations substantially [8].

In the present study, a new reaction rate model is proposed, which is loosely based on the concept of PaSR. The present model utilises the fraction of ignition/interaction mode. Neural network (NN), which has been reported as promising in various combustion modelling approaches [19–24], is employed to predict the reactive structure within the cell. The model is trained, validated and tested with the DNS of MILD combustion, considering both premixed and partially-premixed configurations at various thermo-chemical conditions. The present DNS cases are first described in Section 2. Ignition/interaction mode, which is the key concept for the proposed model, is then introduced in Section 3. Subsequently, the proposed model is described in Section 4. Finally, the developed model is tested and its performance is compared in Section 5.

2. DNS cases

For the present study, the total of five cases of DNS data are used. Three of them, A1, A2 and B1, are premixed cases, whilst two of them, AZ1 and BZ1, are partially premixed cases, as summarised in Table 1. These DNS datasets are explained in this section.

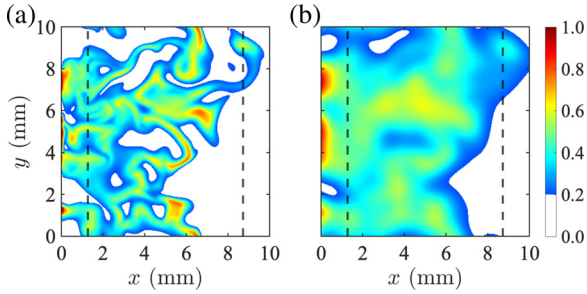

Fig. 1. Instantaneous (a) fully resolved reaction rate and (b) filtered reaction rate ($\Delta = \delta_{th,nom}$) of the case B1 in the mid-xy plane, normalized by using the maximum value. Dashed black lines denotes the sampling domain to avoid the open boundary effect on the filtering.

Table 1
Turbulent combustion conditions of the present DNS data. u' (m/s) is the turbulence intensity and l_0 (mm) is the integral length scale.

	Mode	$\langle X_{O_2,r} \rangle$	u'	l_0
A1	Premixed	0.035	16.4	1.5
A2	Premixed	0.035	10.0	1.7
B1	Premixed	0.025	16.4	1.5
AZ1	Partially premixed	0.035	16.7	1.4
BZ1	Partially premixed	0.025	16.7	1.4

2.1. Premixed cases

The cases A1, A2 and B1 consider MILD combustion under premixed conditions at different turbulence and thermochemical conditions, which have been already reported in previous studies [25]. The reactant mixture is a methane-air premixed mixture with the equivalence ratio of 0.8, which is preheated to 1500 K and also partially mixed with the corresponding burnt mixture to yield the mean oxygen molar fraction $\langle X_{O_2,r} \rangle$ shown in Table 1. The case A1 and A2 yield the same EGR dilution level while higher dilution is considered for the case B1. Also, almost identical turbulent fields are considered for the cases A1 and B1, while a less intense turbulence is considered for the case A2. With these turbulence and thermochemical conditions, the case A2 yields the smallest Karlovitz number Ka among the premixed cases. Also, the case B1 yields largest Ka and most "intense" MILD condition. As described later in Section 4, the case B1 is only used for the testing purpose, but is not used for training of any NN in the present study.

Figure 1 shows a typical variation of the reaction rate ω_c of the reaction progress variable c in the resolved (DNS) and filtered (LES) fields, where a filter size Δ of size equal to the flame thermal thickness δ_{th} is considered. Here, c is defined based on the temperature, and $\omega_c = \Delta H / c_p / (T_b - T_u)$, where ΔH and c_p are respectively heat release rate and specific heat capacity of the mixture. Since in MILD combustion, reaction zones are highly convoluted with a range of localised events (flame propagation, their interaction and ignition) as shown in Fig. 1a, these localised events are considered to yield small length scales compared to typical Δ.

2.2. Partially premixed cases

The cases AZ1 and BZ1 consider MILD combustion under partially premixed conditions with substantial mixture fraction variations, which have been already reported previously [16]. This configuration is more realistic than the cases A1-B1, since most combustion devices utilise separate streams of fuel and oxidiser, which are then mixed for a relatively short time before combustion. Similar to the premixed cases, the partial premixing of fresh non-uniform gas and hot products is also considered, and two different dilution levels are considered as summarised in Table 1. The averaged unburnt temperature is the same as the premixed cases. For AZ1 and BZ1, almost identical turbulent fields are used as a initial and inflowing velocity fields.

For these partially premixed cases, there is additional complexity, where the flame propagation speed and ignition delay are varying locally depending on the local mixture fraction Z. Due to this varying scales, together with their interactions, prediction of SGS reaction rate would be more difficult for the partially premixed cases than that for the premixed cases.

As described later in Section 4, the case BZ1 is only used for the testing purpose, but is not used for the training of any NN in the present study. The present choice of training and testing datasets would make the model assessment more meaningful and rigorous.

2.3. Choice of reference flame quantities

In the following part of the study, various flame quantities are used for the input features of the present NN's. These quantities include thermal flame thickness δ_{th}, unburnt T_u and burnt T_b tem-

peratures, unburnt mixture density ρ_u and flame speed S_L. For the premixed cases, these quantities are uniquely determined for each case, since the mixture fraction Z is almost constant throughout the domain (with very small fluctuation due to differential diffusion effect), and they are computed from the reference laminar flame based on MILD flame element (MIFE) [25]. For the partially premixed cases, these quantities are computed from a tabulation where Z is the control variable. Therefore, these reference flame quantities vary from position to position in the combustion domain. This tabulation is constructed based on various laminar flame solutions at a range of Z values.

Also in the present study, various values of Δ are considered. For reference sake, the considered Δ is normalized by using the "nominal" flame thermal thickness $\delta_{th,nom}$. For the premixed cases, $\delta_{th,nom} = \delta_{th} = 1.3$ mm. For the partially premixed cases, $\delta_{th,nom}(= 3.2$ mm) is obtained from a canonical laminar flame based on the reactant mixture composition obtained by averaging the inhomogeneous mixture fed to the DNS domain. Therefore, each case yield unique $\delta_{th,nom}$ value. Note that $\delta_{th,nom}$ is for reference only, and the choice of its definition does not influence the performance of the present model.

3. Ignition/interaction mode

In the present turbulent combustion model, SGS prediction of ignition/interaction mode is a key. Therefore it is briefly described here. As it is mentioned in the introduction, MILD combustion field may be considered to consist of two types of reaction regions, propagation mode and ignition/interaction mode. The former mode has noticeable scalar gradient $|\nabla c|$, while the latter mode has no significant $|\nabla c|$. However, both modes have similarly high reaction rates ω_c.

Considering such characteristics, the modes can be distinguished separately in the resolved combustion field by comparing ω_c and $|\nabla c|$ values [14]. For instance, threshold values for ω_c and $|\nabla c|$ can be introduced for mode identification. In such manner, ignition/interaction mode can be defined as follows,

$$\Phi(\omega, \psi) = \begin{cases} 1, & \text{if } \omega > \omega^* \text{ and } \psi < \psi^* \\ 0, & \text{otherwise} \end{cases}, \tag{1}$$

where ω^* and ψ^* are the threshold values for ω_c and $|\nabla c|$, respectively. When ω_c is higher and $|\nabla c|$ is lower than their chosen threshold values, the equation gives "1", which represents ignition/interaction mode in the resolved field. Otherwise, the equation gives "0", which means the mixture is either propagating flame or non-reacting zone. In this way, the equation works as a marker for ignition/interaction mode in the resolved combustion field.

Unfortunately, despite the simplicity and intuitiveness of Eq. (1), it could only work with fully resolved fields that may be obtained from DNS or highly-resolved laser measurement images. In other words, Eq. (1) cannot be directly applied for filtered fields in LES, unless very small Δ is considered [26]. When a reasonable Δ is considered, it fails to capture SGS fluctuations, which has significant influence on the local combustion mode of MILD combustion [26]. Also, the threshold values used in Eq. (1) may depend on combustion conditions and Δ of the LES, making them harder to be utilised. In addition to that, the meaning of marker "0" and "1" is rather unclear in unresolved LES fields. For these reasons, it is not practical to implement Eq. (1) for LES directly.

With the above in mind, the filtered combustion mode $\overline{\Phi}_{res}$,

$$\overline{\Phi}_{res} = \overline{\Phi(\omega_c, |\nabla c|)}, \tag{2}$$

can be introduced for LES application. It represents the volume fraction of ignition/interaction mode in a single numerical cell of LES, and it can be obtained by filtering Eq. (1). However, fully resolved fields of ω_c and $|\nabla c|$ are still needed to acquire such quantity. Thus, to avoid using fully resolved fields, which are not available in the LES context, a NN model that can predict $\overline{\Phi}_{res}$ with filtered quantities, $\overline{\omega}_c$ and $|\nabla \tilde{c}|$, has been proposed in a previous study [26]. It can be written as follows:

$$\overline{\Phi}_{NN} = G(\overline{\omega}_c^+, |\nabla \tilde{c}|^+, \Delta^+), \tag{3}$$

where G is a function that represents the NN, and it relates the three input variables in the RHS of Eq. (3) with the filtered combustion mode $\overline{\Phi}_{res}$. Moreover, the subscript "NN" represents quantities predicted by NN, and filtered and Favre filtered quantities are denoted by $\bar{\cdot}$ and $\tilde{\cdot}$, respectively. For the inputs, $\overline{\omega}_c^+$, $|\nabla \tilde{c}|^+$ and Δ^+ are chosen. Note that the superscript "+" denotes normalization of the quantities based on reference laminar flame quantities. In detail, $\overline{\omega}_c$ and $|\nabla c|$ are respectively normalized with $\rho_u S_L/\delta_{th}$ and $1/\delta_{th}$. Meanwhile, Δ is normalized with $2\delta_{th}$. After the normalization, the three inputs become of similar order magnitude, which worked as a feature scaling for the NN.

4. Model description

4.1. Partially stirred reactor (PaSR) model

In PaSR models, it is assumed that each single numerical cell of LES has the reactive structure and the surrounding fluid at the same time [17], and the chemical reactions occur only within the reactive structure. Therefore, the mean reaction rate of the cell predicted by a PaSR model is written as:

$$\overline{\omega}_{c,PaSR} = \kappa \cdot \omega_c^*, \tag{4}$$

where κ and ω_c^* are the fraction of the reactive structure and the reaction rate in the reactive structure, respectively.

Introducing κ, PaSR models can represent imperfect mixing of the reactant gas. It represents the ratio of the reactive structure volume to the cell volume. Usually, κ is calculated with a representative chemical timescale τ_{chem} and a mixing timescale τ_{mix} as follows [18]:

$$\kappa = \frac{\tau_{chem}}{\tau_{chem} + \tau_{mix}}. \tag{5}$$

According to Eq. (5), $\kappa \approx 0$ when $\tau_{mix} \gg \tau_{chem}$, while $\kappa \approx 1$ when $\tau_{mix} \ll \tau_{chem}$. Consequently, PaSR models can consider interaction of chemical and turbulence events. Combination of τ_{chem} and τ_{mix} can be chosen from various types of timescales. For example, combination of τ_{chem} based on the species formation rate and τ_{mix} based on the Z variance and its dissipation rate is proposed for MILD combustion [8]. The choice of these timescales directly affects the accuracy of the PaSR prediction as already reported in [8]. Thus, they need to be carefully selected considering the type of combustion being handled, which could be an ad-hoc process.

As for ω_c^* in Eq. (4), it can be directly obtained from perfectly stirred reactor (PSR) with a residence time τ^* [8,27], or calculated as follows,

$$\omega_c^* = \frac{\overline{\rho}(c^* - c^0)}{\tau^*}, \tag{6}$$

where $\overline{\rho}$, c^*, c^0 and τ^* are mean density, and the reaction progress variables (scalar) in the reactive structure and the surrounding fluid and reactive structure residence time, respectively. c^* can be obtained from PSR or plug flow reactor (PFR), and τ^* is determined as τ_{mix} [18], or $\min(\tau_{mix}, \tau_{chem})$ [8].

4.2. Details of the present neural network model

The proposed NN aided filtered reaction rate model is loosely based on the PaSR approach in terms of assuming reactive structure and surrounding fluids to exist together in a single numerical cell of LES. Thus, $\overline{\omega}_c$ is predicted similarly to Eq. (4). However, to avoid ambiguity in timescale determination, τ^*, τ_{chem} and τ_{mix}, the reactive structure is considered to be a homogeneous reactor, thereby its reaction rate is assumed simply by a zeroth-order approximation $\omega_{c,0th}$ based on GS quantities such as $\tilde{Y}_i$ and $\tilde{T}$. Therefore, the problem of filtered reaction rate prediction now comes down to estimating the volumetric fraction of such homogeneous reactors in the cell on a par with the conventional PaSR. The ways to calculate κ is different in the present study, and also an additional adjustment term f is introduced into the equation as an extension to handle different mixing modes.

In order to predict κ, a NN is implemented and its structure is shown in Fig. 2. The NN computes κ_{NN} with four GS quantities at the position x in a point-wise manner. As shown in Fig. 2, the four inputs for the NN are $\overline{\Phi}_{NN}$, Favre-filtered progress variable $\tilde{c}$, its scalar gradient $|\nabla\tilde{c}|^+$ and Δ^+. The quantities with superscript "+" are being normalised with the reference laminar flame quantities similarly as it is mentioned in Section 3. Among these input features, $\overline{\Phi}_{NN}$ identifies the local combustion mode, which is essentially the balance of chemical source and flux terms as described in Section 3. This quantity is considered to feed some information which acts as an alternative to the chemical and mixing time scales appearing in a conventional PaSR. Therefore, this is considered as a key in the present model. $|\nabla\tilde{c}|^+$ is often used in various SGS models.

In terms of the structures and parameters of the NN, it consists of three fully connected layers. The input layer has four nodes without activation function, while the hidden layer has 50 nodes with ReLU activation function [28]. The output layer has a single node and a sigmoid activation function is considered. This is to bound κ in Eq. (5) between 0 and 1. As for other training parameters, Adam with a learning rate of 10^{-5} is chosen as an optimization algorithm [29], the batch size is set as eight, and the mean squared error is chosen as a loss function. In addition to that, He initialization is used as a weight initialisation [30].

In the present study, f_{NN} is further introduced to consider the local mixing characteristics in the reaction zones, i.e. premixed or non-premixed, and employed in the present modelling as described later in this section. It is obtained with another NN that is depicted in Fig. 2. The NN requires six GS quantities, and the prediction is performed in a point-wise manner on par with the κ_{NN} model. The four of the six quantities are similar to the inputs of the NN that is used for κ_{NN} prediction. The two remaining quantities are Ξ, which is related to the Favre-filtered mixture fraction $\tilde{Z}$, and its scalar gradient $|\nabla\tilde{Z}^+|$. They would represent the extent of premixing of a local region and would be important for partially premixed conditions. In particular, Ξ is defined as $\Xi = \exp(-Z/Z_{st})$, where Z_{st} is the stoichiometric mixture fraction. This helps to identify local compositions, where $\Xi = 1$ for the oxidizer stream, $\Xi \to 0$ for the fuel stream, and $\Xi = 1/e$ for a stoichiometric mixture. Locally lean mixtures yield $1/e < \Xi < 1$ and rich mixtures yield $0 < \Xi < 1/e$. The structure and parameters of the NN is almost similar to the NN model used for κ_{NN} prediction. Therefore, a sigmoid function is introduced as an activation function for the output node, ensuring $0 \leq f_{NN} \leq 1$. The only differences are that the input layer has 6 units, the learning rate of Adam is set as 10^{-4} and the batch size is taken as four.

The separate prediction approach of κ_{NN} and f_{NN} allows flexibility in the choice of training

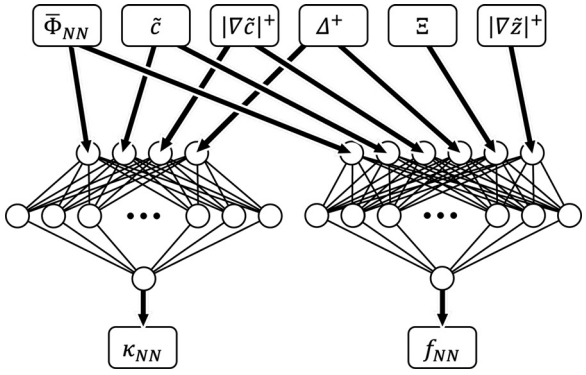

Fig. 2. The NN structures for κ_{NN} and f_{NN} predictions. Corresponding inputs for each NN are also shown, which are normalised based on reference laminar flame quantities.

Table 2
Summary of training and validation (TV) and testing (TE) datasets. Note that $\overline{\Phi}_{NN}$ has been already trained in [26], and not modified in the present study.

	$\overline{\Phi}_{NN}$ [26]	κ_{NN}	f_{NN}	$\overline{\omega}_{c,NN}$
A1	TV	TV	TV	-
A2	TV	TV	TV	-
B1	TE	-	-	TE
AZ1	-	-	TV	-
BZ1	-	-	-	TE

datasets, i.e. it allows the use of imbalanced training data between premixed and non-premixed combustion data for κ_{NN}, which has a great impact on the overall model performance. In fact, the present κ_{NN} is trained by only using premixed cases and successfully applied to the partially premixed test case as discussed in Section 5.

For the training of the NN for κ_{NN} prediction, the target quantity is computed as $\overline{\omega}_{c,DNS}/\omega_{c,0th}$, which represents the true κ. Here, $\omega_{c,0th}$ is the zeroth-order approximated reaction rate, as described later in this section. Also, $\overline{\omega}_{c,DNS}$ is the "correct" value of the filtered reaction rate obtained directly from the DNS data using a Gaussian filtering, along with other input quantities. Similarly, $\overline{\omega}_{c,DNS}/(\kappa_{NN}\cdot\omega_{c,0th})$ is set as the target for the training of the NN for f_{NN}. It represents the adjustment term for κ based on the local mixing mode.

The choice of training, validation and testing datasets are summarised in Table 2. A total of 22,104 samples from the case A1 and A2 at nine different snapshots and four different filter sizes Δ are used for training of the NN for κ_{NN}, while 5238 samples from the case A1, A2 and AZ1 at three different snapshots and four different filter sizes Δ are used for the training for f_{NN}.

Finally, for ω_c^* in Eq. (4), a zeroth-order approximation of the reaction rate $\omega_{c,0th}$ is used ($\omega_c^* = \omega_{c,0th}$), by assuming a sufficiently small residence time (integration time) τ^*. Therefore, $\omega_{c,0th}$ is computed based on a chosen kinetic mechanism by simply substituting the corresponding GS quantities for inputs. Subsequently, κ_{NN}, f_{NN} and $\omega_{c,0th}$ are multiplied in order to acquire the prediction of an SGS reaction rate $\overline{\omega}_{c,NN}$ in a similar manner to Eq. (4) as:

$$\overline{\omega}_{c,NN} = \kappa_{NN}\cdot f_{NN}\cdot\omega_{c,0th}. \tag{7}$$

Note that for the prediction of $\overline{\Phi}_{NN}$, $\overline{\omega}_c^+$ is required as an input. For the ultimate purpose of $\overline{\omega}_c^+$ prediction, this looks a circular reference and it is not desirable. However, as tested and described in Section 5.2, the input $\overline{\omega}_c^+$ for $\overline{\Phi}_{NN}$ can be obtained from the previous time step in an actual LES.

5. Results and discussion

In this section, the performance of the proposed model is tested, and the model's sensitivity to Φ_{NN} is investigated.

5.1. Model performance

As visual evaluation of the proposed model, the mid-xy plane of the instantaneous $\overline{\omega}_{c,NN}^+$ and $\overline{\omega}_{c,DNS}$ fields are compared for different Δ for the cases B1 and BZ1. Figure 3 shows $\overline{\omega}_{c,NN}$ and $\overline{\omega}_{c,DNS}^+$ of the case B1 for four different Δ, ranging from $0.5\delta_{th,nom}$ to $2\delta_{th,nom}$. It is clear that the model could predict reasonably well for all Δ considered. The similar performance is obtained for prediction of the case BZ1 as shown in Fig. 4. This is also supported by the correlation of prediction and target values shown in Fig. 5.

The Pearson's correlation coefficient r_P and mean squared error (MSE) ε_{MSE} between $\overline{\omega}_{c,NN}^+$ and $\overline{\omega}_{c,DNS}^+$ are examined for the quantitative model assessment (denoted as NN/DNS). Also, for the purpose of quantifying the SGS activities, r_P and

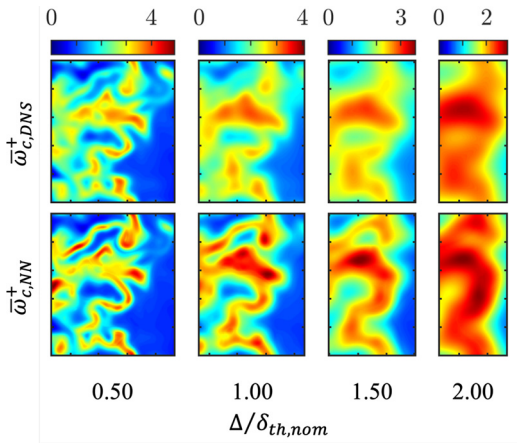

Fig. 3. Typical comparison of $\overline{\omega}^+_{c,DNS}$ and $\overline{\omega}^+_{c,NN}$ for $\Delta/\delta_{th,nom} = 0.50, 1.00, 1.50, 2.00$ for the case B1.

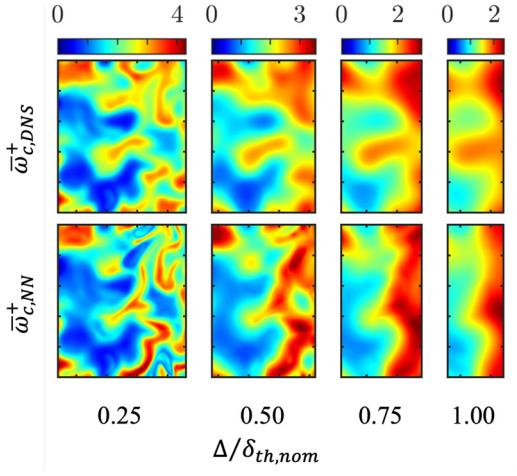

Fig. 4. Typical comparison of $\overline{\omega}^+_{c,DNS}$ and $\overline{\omega}^+_{c,NN}$ for $\Delta/\delta_{th} = 0.25, 0.5, 0.75, 1.00$ for the case BZ1.

ε_{MSE} between $\omega^+_{c,0th}$ and $\overline{\omega}^+_{c,DNS}$ are computed (denoted as 0th/DNS).

The calculated r_P is shown in Fig. 6 for a range of Δ, and r_P shows relatively higher values, which are over 0.79 for 0th/DNS, and over 0.90 for NN/DNS. Generally, r_P decreases with increasing Δ for both NN/DNS and 0th/DNS due to the increasing contribution from SGS, except for NN/DNS for the case BZ1. The value of r_P of 0th/DNS relatively high for the prediction of the case BZ1, and it is higher than that of NN/DNS for $\Delta/\delta_{th,nom} = 0.25$ for the case BZ1. This *falsely* suggests that the zeroth-order approximation $\omega_{c,0th}$ yields equal or better prediction performance compared to $\overline{\omega}_{c,NN}$ for some conditions. However, as described next, the correlation coefficient alone is not a definitive quantification of the model performance, since it only accounts for the "trend" of the predicted distribution. Nevertheless, relatively high r_P for 0th/DNS suggests that the use of PaSR equation in Eq. (4) is promising only if κ is appropriately predicted, which is the objective in the present study.

To complement the lack of r_P as a quantification of model performance, ε_{MSE} for NN/DNS and 0th/DNS is also computed and shown in Fig. 7. Clearly, for all the cases and Δ, the error is substantially lower for the present NN model $\overline{\omega}_{c,NN}$ (Eq. (7)) than the zeroth-order approximation $\omega_{c,0th}$, suggesting that SGS contribution is well taken into account in the present NN model. The comparison of r_p and ε_{MSE} also suggests that the prediction of κ in Eq. (4) is pivotal in the PaSR approaches, and the present model's approach $\kappa = \kappa_{NN} \cdot f_{NN}$ does this successfully.

The filtered reaction rate is also predicted by using a conventional PaSR method for further comparison. There are various choices of submodels required to compute Eq. (4), and here is the present choice. The reaction rate of the reactive structure, ω^*_c, is directly obtained from the PSR [8,27] with the residence time $\tau^* = \tau_{mix}$ [18]. The chemical and mixing timescales, τ_{chem} and τ_{mix}, are computed as $\tau_{chem} = \max[Y^*_i/(dY^*_i/dx)]$ and $\tau_{mix} = \sqrt{\tau_\Delta \tau_\eta}$ [7]. Here, the quantities of the reactive structure (super-

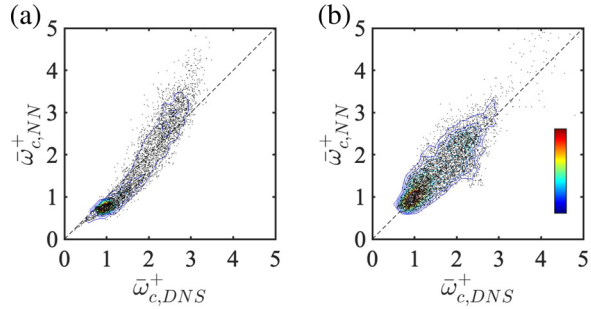

Fig. 5. Joint PDF and scatters between $\overline{\omega}_{c,NN}$ and $\overline{\omega}_{c,DNS}$ for the cases (a) B1 and (b) BZ1.

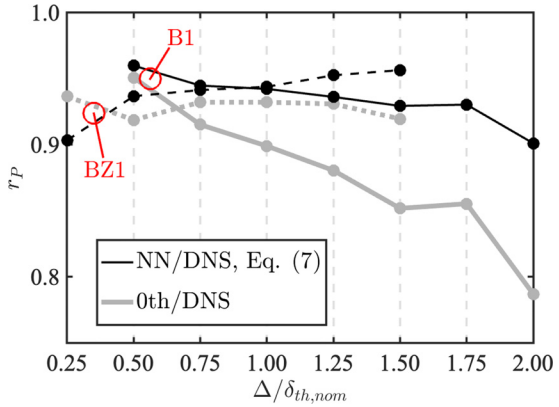

Fig. 6. Pearson correlation coefficients r_P computed for NN/DNS (black) and 0th/DNS (grey) obtained for the cases B1 (solid line) and BZ1 (dashed line). $\Delta/\delta_{th,nom} = 0.25, 0.50, \cdots, 2.00$. r_P is computed by using nine different snapshots for each filter sizes for the case B1, while three snapshots are considered for the case BZ1.

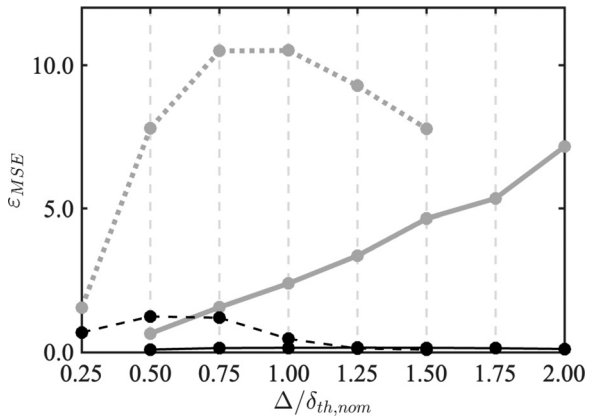

Fig. 7. Mean squared errors ε_{MSE} computed for NN/DNS and 0th/DNS for the cases B1 and BZ1. For the sampling method and the line legend, see Fig. 6.

script "*") are computed by using PSR. Also, $\tau_\Delta = \Delta/u'$ and $\tau_\eta = \sqrt{\nu/\epsilon_\Delta}$, where $\epsilon_\Delta = u'^3/\Delta$. Since the present prediction is performed in the a priori context, u' is directly obtained from the DNS results. However, in the actual LES simulations, this quantities needs to be also estimated by using an appropriate submodel. The correlation coefficient r_P of the predicted and DNS values ranges between 0.57–0.60 for the case B1 and 0.74–0.88 for the case BZ1 for the filter sizes considered in Fig. 6.

5.2. Features of predicted reactive structure

Figure 8 shows typical instantaneous fields of $\overline{\omega}_{NN}$, κ_{NN}, f_{NN} and $\overline{\Phi}_{NN}$ predicted by the NN models. As described in Section 4.2, κ_{NN} does not exactly equal to κ in the conventional PaSR in Eq. (4). However, there are some similarities between the variations of κ_{NN} and $\overline{\omega}_{c,NN}$ for the premixed case of B1. This suggests that κ_{NN} is still the key in $\overline{\omega}_{c,NN}$ prediction on a par with κ in the conventional PaSR. Also, a similar relationship can be observed for κ_{NN} and $\overline{\Phi}_{NN}$ for the case B1. This suggests that the local combustion mode is useful for the local reactive structure prediction. These local correlations between $\overline{\omega}_{c,NN}$ and κ_{NN}, and κ_{NN} and $\overline{\Phi}_{NN}$ are less obvious for the non-premixed case of the case BZ1. This is considered predominantly due to the local mixing effect of fuel and oxidizer, which is separately treated by f_{NN}. Indeed, f_{NN} ranges larger values for the case BZ1 than B1, suggesting that there is additional complexity due to the imperfect mixing and this is handled well by f_{NN}.

5.3. Sensitivity of $\overline{\Phi}_{NN}$ on prediction of $\overline{\omega}_c$

As noted in Section 4.2, the prediction of $\overline{\Phi}_{NN}$ requires $\overline{\omega}_c$ as an input, which is not possible in an actual LES. What can be done is that the reaction rate at the previous time step is used instead of $\overline{\omega}_c$ as an input for the prediction of $\overline{\Phi}_{NN}$. Denoting the reaction rate at the previous time step by $\overline{\omega}_c^*$, there

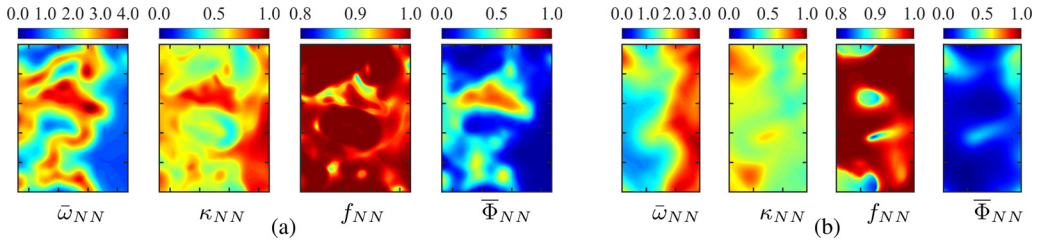

Fig. 8. Typical variations of $\overline{\omega}_{NN}$, κ_{NN}, f_{NN} and $\overline{\Phi}_{NN}$ for B1 (a; $\Delta/\delta_{th,nom} = 1.0$) and BZ1 (b; $\Delta/\delta_{th,nom} = 0.75$).

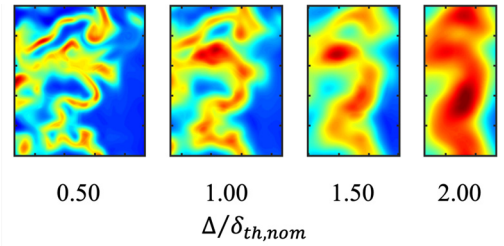

Fig. 9. Variation of $\overline{\omega}^{\delta z}_{c,NN}$, in which $\overline{\Phi}_{NN}$ is calculated with $\overline{\omega}^{\delta z}_{c}$ for different $\Delta/\delta_{th,nom}$. Compare with Fig. 3 to see the effect of ϵ_{ω} on $\overline{\omega}_{c,NN}$.

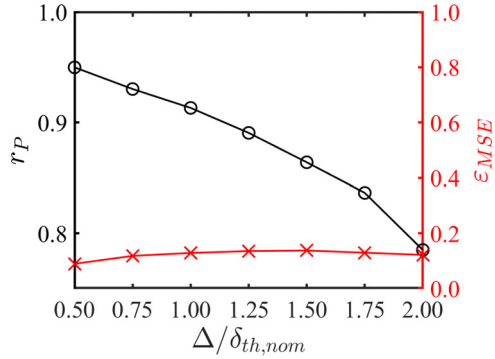

Fig. 10. Corresponding r_P (○) and ϵ_{mse} (×) of the $\overline{\omega}^{\delta z}_{c,NN}$ field shown in Fig. 9 at different Δ.

is a difference between the reaction rates from the two consecutive snapshots $\varepsilon_{\omega} = |\overline{\omega}_c - \overline{\omega}^*_c|$. Due to the Courant-Friedrichs-Lewy (CFL) condition, ε_{ω} is expected to be relatively small, but the sensitivity of ε_{ω} in the input of the $\overline{\Phi}_{NN}$ for the prediction of $\overline{\omega}_{c,NN}$ needs to be assessed. Also, such an assessment would explain the effect of uncertainty propagation from $\overline{\Phi}_{NN}$ to $\overline{\omega}_c$ via κ_{NN}.

In the context of *a priori* assessment, $\overline{\omega}^*_c$ is impossible to obtain. Instead, $\overline{\omega}^*_c$ is substituted by $\overline{\omega}^{\delta z}_c$ in this study. Here, $\overline{\omega}^{\delta z}_c$ is $\overline{\omega}_c$ sampled from a neighbouring z plane whose z position is different by δz from the plane at which all other quantities are sampled. Here, $\delta z = 0.5\Delta$ is considered. We assume that $\varepsilon_{\omega} \sim |\overline{\omega}_c - \overline{\omega}^{\delta z}_c|$. Also, $\delta z = 0.5\Delta$ is considered to be sufficient for this assessment due to the CFL condition (i.e. $\Delta \gg U\Delta t$) in an LES.

Figure 9 shows the prediction of $\overline{\omega}^{\delta z}_{c,NN}$ at different Δ considering $\overline{\omega}^{\delta z}_c$ as the input for Φ_{NN}. Comparing with Fig. 3, it is clear that ε_{ω} results in only slight deviation in the predicted field. For a more quantitative assessment, r_P and ε_{MSE} are shown for $\overline{\omega}^{\delta z}_{c,NN}$ at different Δ in Fig. 10. While ε_{MSE} shows only slight increase, r_P progressively decreases with Δ compared to Fig. 6. This is because the "shift" of the z-plane δz increases with Δ. To improve the model at larger Δ, $\overline{\omega}_c$ can be iteratively obtained: the predicted $\overline{\omega}_c$ from the first iteration can be fed again to yield better prediction of $\overline{\Phi}_{NN}$. Nevertheless, given $r_P \gtrsim 0.8$ and a relatively small ε_{MSE} compared to the one for the zeroth-order approximation shown in Fig. 7, it is expected that the use of $\overline{\omega}^*_c$ would not unduly influence the performance of the proposed model, and this strategy is applicable for an actual LES without reducing the model performance.

6. Conclusions

A filtered reaction rate model has been developed for MILD combustion. The framework of the present model is based on the PaSR approach. The fraction of the reactive structure is predicted using two separate NN's, to consider both premixed and non-premixed conditions, while allowing the use of imbalanced training data between premixed and non-premixed combustion DNS data. The training of these NN's are carried out by using DNS data of premixed and partially premixed MILD combustion. The key ingredient in the present model is the use of the local combustion mode prediction performed by using another NN, which was developed in a previous study.

The trained model was then assessed by using two unknown combustion DNS cases, which yields much higher dilution level (more intense MILD condition) and a higher Ka than the DNS cases used for training. The model assessment has been carried out by means of the Pearson's correlation coefficient and mean squared error.

For both the present model and zeroth-order approximated reaction rate, the correlation coeffi-

cient shows relatively high values, suggesting that the trend of predicted field, by the present model and zeroth-order approximation, is well correlated with the actual reaction rate field. This suggests that the use of the PaSR equation is promising only if the fraction of the reactive structure is appropriately predicted, which is the objective in the present study. On the other hand, substantially lower mean squared error is observed for a range of filter sizes for both premixed and partially premixed cases for the proposed NN model than that for the zeroth-order approximation. The comparison of the predicted fields by the three NN suggests that the local combustion mode is useful for the local reactive structure prediction. These results suggest that the present NN approach works well in the prediction of MILD combustion despite the imbalanced training datasets. Future work should investigate whether this holds for prediction of Y_i species as well.

Declaration of Competing Interest

The authors declare that they have no known competing financial interests or personal relationships that could have appeared to influence the work reported in this paper.

Acknowledgments

Y.M. acknowledges the supports of JSPS Grant-in-Aid for Young Scientists (B) Grant Number 19K14903 and JST, PRESTO Grant Number JPMJPR21OB. K.J. acknowledges the support of Japanese Government (MEXT) Scholarship for Research Students. This work made use of the TSUBAME3.0 supercomputer at Tokyo Institute of Technology.

References

[1] J.A. Wünning, J.G. Wünning, Flameless oxidation to reduce thermal no-formation, Prog. Energy Combust. Sci. 23 (1997) 81–94.
[2] M. Katsuki, T. Hasegawa, The science and technology of combustion in highly preheated air, Proc. Combust. Inst. 27 (2) (1998) 3135–3146.
[3] A. Cavaliere, M. de Joannon, Mild combustion, Prog. Energy Combust. Sci. 30 (2004) 329–366.
[4] C. Duwig, D. Stankovic, L. Fuchs, G. Li, E. Gutmark, Experimental and numerical study of flameless combustion in a model gas turbine combustor, Combust. Sci. Technol. 180 (2) (2008) 279–295.
[5] M. Ihme, L. Shunn, J. Zhang, Regularization of reaction progress variable for application to flamelet-based combustion models, J. Comput. Phys. 231 (23) (2012) 7715–7721.
[6] Z. Chen, V.M. Reddy, S. Ruan, N.A. Doan, W.L. Roberts, N. Swaminathan, Simulation of MILD combustion using Perfectly Stirred Reactor model, Proc. Combust. Inst. 36 (3) (2017) 4279–4286.
[7] Z. Li, A. Cuoci, A. Parente, Large Eddy Simulation of MILD combustion using finite rate chemistry: effect of combustion sub-grid closure, Proc. Combust. Inst. 37 (4) (2019) 4519–4529.
[8] S. Iavarone, A. Péquin, Z.X. Chen, N.A.K. Doan, N. Swaminathan, A. Parente, An a priori assessment of the partially stirred reactor (PASR) model for mild combustion, Proc. Combust. Inst. 38 (4) (2021) 5403–5414.
[9] T. Plessing, N. Peters, J.G. Wünning, Laseroptical investigation of highly preheated combustion with strong exhaust gas recirculation, Proc. Combust. Inst. 27 (2) (1998) 3197–3204.
[10] I.B. Özdemir, N. Peters, Characteristics of the reaction zone in a combustor operating at mild combustion, Exp. Fluids 30 (6) (2001) 683–695.
[11] B.B. Dally, E. Riesmeier, N. Peters, Effect of fuel mixture on moderate and intense low oxygen dilution combustion, Combust. Flame 137 (4) (2004) 418–431.
[12] N. Krishnamurthy, P.J. Paul, W. Blasiak, Studies on low-intensity oxy-fuel burner, Proc. Combust. Inst. 32 (II (2)) (2009) 3139–3146.
[13] J. Sidey, E. Mastorakos, Visualization of MILD combustion from jets in cross-flow, Proc. Combust. Inst. 35 (3) (2015) 3537–3545.
[14] Y. Minamoto, T.D. Dunstan, N. Swaminathan, R.S. Cant, DNS of EGR-type turbulent flame in MILD condition, Proc. Combust. Inst. 34 (2) (2013) 3231–3238.
[15] Y. Minamoto, N. Swaminathan, S.R. Cant, T. Leung, Morphological and statistical features of reaction zones in MILD and premixed combustion, Combust. Flame 161 (11) (2014) 2801–2814.
[16] N.A.K. Doan, N. Swaminathan, Y. Minamoto, DNS of MILD combustion with mixture fraction variations, Combust. Flame 189 (2018) 173–189.
[17] J. Chomiak, Combustion A Study in Theory, Fact and Application, Abacus Press/Gordon and Breach Science Publishers, New York, 1990.
[18] P.A. Nordin, Complex chemistry modeling of diesel spray combustion, Chalmers University of Technology, Chalmers, Sweden, 2001 Ph.D. thesis.
[19] M. Ihme, C. Schmitt, H. Pitsch, Optimal artificial neural networks and tabulation methods for chemistry representation in LES of a bluff-body swirl-stabilized flame, Proc. Combust. Inst. 32 (1) (2009) 1527–1535.
[20] Z.M. Nikolaou, C. Chrysostomou, L. Vervisch, S. Cant, Progress variable variance and filtered rate modelling using convolutional neural networks and flamelet methods, Flow Turbul. Combust. 103 (2019) 485–501.
[21] C.J. Lapeyre, A. Misdariis, N. Cazard, D. Veynante, T. Poinsot, Training convolutional neural networks to estimate turbulent sub-grid scale reaction rates, Combust. Flame 203 (2019) 255–264.
[22] S. Yellapantula, M.T.H. de Frahan, R. King, M. Day, R. Grout, H. Pitsch, Machine learning of combustion LES models from reacting direct numerical simulation, in: A. Attili (Ed.), Data analysis for direct numerical simulations of turbulent combustion, Springer International Publishing, 2020, pp. 273–292.
[23] Z.X. Chen, S. Iavarone, G. Ghiasi, V. Kannan, G. D'Alessio, A. Parente, N. Swaminathan, Application of machine learning for filtered density function

closure in MILD combustion, Combust. Flame 225 (2020) 160–179.
[24] R. Nakazawa, Y. Minamoto, N. Inoue, M. Tanahashi, Species reaction rate modelling based on physics-guided machine learning, Combust. Flame 235 (2022) 111696.
[25] Y. Minamoto, N. Swaminathan, Scalar gradient behaviour in MILD combustion, Combust. Flame 161 (4) (2014) 1063–1075.
[26] K. Jigjid, C. Tamaoki, Y. Minamoto, R. Nakazawa, N. Inoue, M. Tanahashi, Data driven analysis and prediction of MILD combustion mode, Combust. Flame 223 (2021) 474–485.
[27] Z. Li, S. Tomasch, Z.X. Chen, A. Parente, I.S. Ertesvåg, N. Swaminathan, Study of MILD combustion using LES and advanced analysis tools, Proc. Combust. Inst. 38 (4) (2021) 5423–5432, doi:10.1016/j.proci.2020.06.298.
[28] X. Glorot, A. Bordes, Y. Bengio, Deep sparse rectifier neural networks, Int. Conf. Artif. Intell. Stat. AISTATS 2011 (15) (2011) 315–323.
[29] D.P. Kingma, J.L. Ba, Adam: A method for stochastic optimization, in: 3rd Int. Conf. Learn. Represent, ICLR 2015 - Conf. Track Proc., 2015, pp. 1–15.
[30] K. He, X. Zhang, S. Ren, J. Sun, Delving deep into rectifiers: Surpassing human-level performance on imagenet classification, in: Proc. IEEE Int. Conf. Comput. Vis., 2015, 2015.